Development/Plasticity/Repair

Preserved Motility after Neonatal Dopaminergic Lesion Relates to Hyperexcitability of Direct Pathway Medium Spiny Neurons

Ettel Keifman,[*] Camila Coll,[*] Cecilia Tubert, Rodrigo M. Paz, Juan E. Belforte, Mario G. Murer, and Barbara Y. Braz

Universidad de Buenos Aires, CONICET, Instituto de Fisiología y Biofísica Bernardo Houssay, Grupo de Neurociencia de Sistemas, 2155 Paraguay St, Buenos Aires, 1121, Argentina

In Parkinson's disease patients and rodent models, dopaminergic neuron loss (DAN) results in severe motor disabilities. In contrast, general motility is preserved after early postnatal DAN loss in rodents. Here we used mice of both sexes to show that the preserved motility observed after early DAN loss depends on functional changes taking place in medium spiny neurons (MSN) of the dorsomedial striatum (DMS) that belong to the direct pathway (dMSN). Previous animal model studies showed that adult loss of dopaminergic input depresses dMSN response to cortical input, which likely contributes to Parkinson's disease motor impairments. However, the response of DMS-dMSN to their preferred medial PFC input is preserved after neonatal DAN loss as shown by *in vivo* studies. Moreover, their response to inputs from adjacent cortical areas is increased, resulting in reduced cortical inputs selectivity. Additional *ex vivo* studies show that membrane excitability increases in dMSN. Furthermore, chemogenetic inhibition of DMS-dMSN has a more marked inhibitory effect on general motility in lesioned mice than in their control littermates, indicating that expression of normal levels of locomotion and general motility depend on dMSN activity after early DAN loss. Contrastingly, DMS-dMSN inhibition did not ameliorate a characteristic phenotype of the DAN-lesioned animals in a marble burying task demanding higher behavioral control. Thus, increased dMSN excitability likely promoting changes in corticostriatal functional connectivity may contribute to the distinctive behavioral phenotype emerging after developmental DAN loss, with implications for our understanding of the age-dependent effects of forebrain dopamine depletion and neurodevelopment disorders.

Key words: corticostriatal system; development; dopamine; *in vivo* recordings; medium spiny neurons; striatum

---

Significance Statement

The loss of striatal dopamine in the adult brain leads to life-threatening motor impairments. However, general motility remains largely unaffected after its early postnatal loss. Here, we show that the high responsiveness to cortical input of striatal neurons belonging to the direct basal ganglia pathway, crucial for proper motor functioning, is preserved after early dopamine neuron loss, in parallel with an increase in these cells' membrane excitability. Chemogenetic inhibition studies show that the preserved motility depends on this direct pathway hyperexcitability/hyperconnectivity, while other phenotypes characteristic of this condition remained unaltered despite the dMSN inhibition. This insight has implications for our understanding of the mechanism underlying the behavioral impairments observed in neuropsychiatric conditions linked to early dopaminergic hypofunction.

Introduction

The basal ganglia (BG) are a group of subcortical nuclei involved in voluntary motor control and several aspects of behavior and learning (Balleine, 2019; Peak et al., 2020). Dopamine is a key regulator of cortical information flow through the striatum, the main input nucleus of the BG, and its influence during postnatal development is crucial for the proper maturation of corticostriatal function (Galiñanes et al., 2009; Braz et al., 2015; Lieberman et al., 2018). Corticostriatal and nigrostriatal synapses experience a marked maturation during infancy and adolescence in rodents and humans (Hattori and McGeer, 1973;

Stamford, 1989; Teicher et al., 1995; Sharpe and Tepper, 1998; Montague et al., 1999; Castellanos, 2002; Peixoto et al., 2019; Larsen et al., 2020) and many studies link early dopaminergic perturbations to neuropsychiatric conditions, such as attention deficit hyperactivity disorder, autism, and Tourette syndrome (Castellanos and Tannock, 2002; Biederman and Faraone, 2005; Durston et al., 2005; Mazei-Robison et al., 2005; Volkow et al., 2007; Hamilton et al., 2013; Bowton et al., 2014; Maia and Conceição, 2018; Vicente et al., 2020). The elucidation of the mechanisms that regulate corticostriatal circuit development is crucial to understand the pathophysiology of these disorders.

Dopamine differentially regulates the activity of the two main populations of striatal medium spiny neurons (MSNs) that give rise to the direct and indirect BG pathways (Gerfen and Surmeier, 2011). Direct pathway MSNs (dMSNs) express the excitatory dopamine D1 receptor, whereas indirect pathway MSNs (iMSNs) express inhibitory dopamine D2 receptors. In addition, the dorsal striatum is functionally organized into two main territories that interact with each other through re-entrant cortico-BG-thalamocortical circuits (Voorn et al., 2004; Pennartz et al., 2009; Hintiryan et al., 2016): the dorsolateral striatum (DLS), which receives inputs mainly from sensorimotor cortices and supports motor performance and automatized behavior, and the dorsomedial striatum (DMS), which receives inputs preferentially from the PFC and supports flexible goal-directed behavior, exploration, and response to novelty (Balleine and Dickinson, 1998; Packard and Knowlton, 2002; Daw et al., 2005; Yin and Knowlton, 2006; Graybiel, 2008; Jin and Costa, 2015). For instance, the DMS regulates spontaneous locomotion, whereas dMSNs and iMSNs promote and inhibit ambulation, respectively (Durieux et al., 2009; Kravitz et al., 2010). Moreover, DMS dMSNs are markedly hypoactive in parkinsonian animals (Parker et al., 2018; Ryan et al., 2018), and optogenetic activation of DMS dMSN rescues locomotor activity in mice rendered parkinsonian by lesioning the nigrostriatal pathway (Kravitz et al., 2010). Strikingly, spontaneous locomotion is preserved or even increased in mice whose midbrain dopaminergic neurons (DANs) have been injured early after birth (Shaywitz et al., 1976; Avale et al., 2004a; Galiñanes et al., 2009) or failed to develop because of gene mutations (Eells et al., 2002; Nunes et al., 2003; Filali and Lalonde, 2016; del Río-Martín et al., 2019; Montarolo et al., 2019), likely thanks to nondopaminergic compensations since general motility in these animal models is resistant to administration of dopamine receptor antagonists (Bruno et al., 1985; Duncan et al., 1987; Ardayfio et al., 2010). Why locomotor activity is preserved in these animal models remains unknown.

Since dMSN activity stimulates locomotion and their depressed activity is partially responsible for the characteristic hypokinesia and bradykinesia that follows the degeneration of already established nigrostriatal dopaminergic projections in the adult (Kravitz et al., 2010; Escande et al., 2016; Parker et al., 2018; Ryan et al., 2018), we asked whether functional adaptations rescue dMSN activity and consequently locomotion when the nigrostriatal projection is ablated early after birth, well before it completes its development (Voorn et al., 1988; Stamford, 1989; Ferrari et al., 2012; Larsen et al., 2020).

Materials and Methods
Animals
Drd1a-tomato (Shuen et al., 2008) and *D1-Cre* (B6.FVB(Cg)-Tg(Drd1-cre)EY262Gsat/Mmucd, RRID:MMRRC_030989-UCD) transgenic mice were maintained under a 12 h light:12 h dark cycle with *ad libitum*

access to food and water and cared for in accordance with institutional (Institutional Animal Care and Use Committee, RS2964/2010 and 2598/13, University of Buenos Aires) and government regulations (SENASA, RS617/2002). All efforts were made to minimize the number of animals used and their suffering.

Neonatal DAN lesion
Neonatal dopamine neuron lesions were done as previously described (Avale et al., 2004b; Braz et al., 2015). Before surgery, pups were observed with a fluorescent lamp and selected if red fluorescence was seen in their brain hemispheres. PD2 pups received bilateral injections of the catecholaminergic neurotoxin 6-hydroxydopamine (6-OHDA-HBr, 1.52 µl per ventricle of an 8.33 mg/ml solution; Sigma) or vehicle (0.1% ascorbic acid) in each lateral ventricle (1.1 mm below the skin, 0.6 mm from midline, and 1.5 mm anterior to the λ) under hypothermal anesthesia, after desipramine pretreatment 30 min before the lesion (20 mg/kg, s.c.) to protect noradrenergic neurons. Injections were performed at a constant rate of 1.25 µl/min with a 30 gauge needle coupled to a 25 µl Hamilton syringe driven by a microinfusion pump (Bee syringe pump and controller, Bioanalytical Systems). In each litter, half of the pups received the toxin and the other half vehicle. After surgery, they were warmed up and returned to their home cages in groups of up to 8 pups per breastfeeding mother until weaning (PD24). Thereafter, control and lesion mice were housed together in the same cage in groups of 4-6 until the electrophysiological experiment (12-30 weeks). All the neonatal dopaminergic lesions were confirmed postmortem by immunohistochemical detection of TH (described in Histology and immunohistochemistry). Representative examples of immunostained histologic sections are shown in Figure 5C.

In vivo *electrophysiological recordings*
All recordings were performed under urethane anesthesia (1.2-1.5 g/kg i.p.) following published protocols (Braz et al., 2015; Escande et al., 2016). Local anesthetic (bupivacaine hydrochlorate solution, 5% v/v, Durocaine, AstraZeneca) was applied subcutaneously on the scalp (0.05 ml), and the animal was affixed to a stereotaxic frame (Stoelting). Body temperature was maintained at 36°C-37°C with a servocontrolled heating pad (Fine Science Tools). During the experiment, the level of anesthesia was regularly verified by testing the nociceptive hindlimb withdrawal reflex and by online visual examination of the frontal cortex electrocorticogram. Supplemental doses of urethane were customarily given throughout the experiment (0.3 g/kg s.c. every 2-3 h).

Cortical electrical stimulation. In all experiments, a concentric bipolar electrode (SNE-100, Better Hospital Equipment; outer contact diameter 0.25 mm, central contact diameter 0.1 mm, contacts separation 0.75 mm, contact exposure 0.25 mm) was placed into the prelimbic (Prl) area of the mPFC (2.0 mm anterior to bregma, 0.4 lateral to midline, 2.0 mm ventral to the cortical surface, ipsilateral to the striatal recording site) according to Paxinos and Franklin (2004). To study striatal responses evoked by stimulation of different cortical areas, we placed an additional concentric bipolar electrode in the cingulate/secondary motor (Cg/M2) cortex (2.0 mm anterior to bregma, 0.8 mm lateral, 1.2 mm ventral). Stimulus–response curves to cortical stimulation were obtained with stimuli consisting of 300 µs square pulses (Iso-Flex and Master 8, AMPI) applied every 4 s, 40 times at each current intensity (100-800 µA).

Juxtacellular recordings of DMS-MSN. Juxtacellular recordings of striatal neurons were performed in *Drd1a-tomato* mice. The following stereotaxic coordinates were used: 0.8 mm from bregma, 1.2-1.6 mm from the midline with a 10° angle in the coronal plane, and 2-2.5 mm below the brain surface. Recordings were obtained with glass microelectrodes with a tip diameter of 1-2 µm (14-25 MΩ) filled with 2% Neurobiotin (Vector Laboratories) in 0.5 M NaCl. Electrode signal was sent to an Axoclamp 2B amplifier (Molecular Devices) and digitized at 20 kHz using a DigiData 1332 A/D board system and digitally filtered (100 Hz to 5 kHz, Axoscope 9.0; Molecular Devices). Because MSNs are silent or fire at very low rates, they were detected by evoking orthodromic responses by stimulating the Prl cortex every 2 s at 700 µA while the recording electrode descended slowly through the striatum. To label the recorded cells (Pinault, 1996; Escande et al., 2016), positive current

pulses (500 ms at 2 Hz) driving spike discharges (3-15 nA) were delivered through the recording electrode for 5-15 min.

Ex vivo *electrophysiological recordings*

Acute slice preparation. Mice were anesthetized with isoflurane and decapitated. The brain was quickly removed, chilled in ice-cold low Ca^{2+}-high Mg^{2+} aCSF, and prepared for slicing; 300-μm-thick coronal slices at the level of the striatum were cut by using a vibratome (Pelco T series 1000, Ted Pella). Slices were submerged in low Ca^{2+}-high Mg^{2+} aCSF at 34°C for 30 min and then kept in the same aCSF at room temperature in a recovery chamber. aCSF composition was as follows (in mM): 125 NaCl, 2.5 KCl, 1.3NaH$_2$PO$_4$·H$_2$O, 26 NaHCO$_3$, 2 CaCl$_2$, 1 MgCl$_2$, and 10 glucose. For low-Ca^{2+}-high-Mg^{2+} aCSF, 0.5 mM CaCl$_2$ and 2.5 mM MgCl$_2$ were used.

Whole-cell recordings. Slices were transferred to a submersion-type chamber perfused by a peristaltic pump (Ismatec) with aCSF at a constant rate of 3 ml/min; temperature in the recording chamber was set at 34°C with a TC-344B temperature controller (Warner Instruments). Cells were visualized using an upright microscope (Nikon Eclipse) equipped with a 40× water-immersion objective, DIC and fluorescent optics, and an infrared camera connected to a monitor and computer. Recording electrodes were made with borosilicate glass capillaries shaped with a puller (P-97, Sutter Instruments). For whole-cell recordings, electrodes were filled with internal solution containing the following (in mM): 20 KCl, 120 K-gluconate, 10 HEPES, 3 Na$_2$ATP, 0.3 NaGTP, 0.1 EGTA, 10 phosphocreatine, and 2 MgCl$_2$, pH 7.3 adjusted with KOH. Neurobiotin was included in the intracellular solution for all the recordings. Recordings were amplified (Axopatch-1D; Molecular Devices), sampled at 20 kHz (Digidata 1322A, Molecular Devices), and acquired on a PC running pClamp 9.2 (Molecular Devices).

For the analysis of dMSN excitability after hM4D(Gi)-mCherry-DIO activation, *ex vivo* brain slices were perfused with aCSF containing picrotoxin (100 μM), CNQX (20 μM), and clozapine-N-oxide (CNO, 5 μM).

Analysis of electrophysiological data

In vivo recordings. Data analysis was performed with ClampFit (Molecular Devices). We studied the evoked responses by stimulating the Prl cortex every 4 s at increasing current intensities (100-800 μA, 100 μA steps, 0.3 ms square wave pulse duration, 40 trials per stimulation intensity) and then applying the same stimulation protocol to study the response to Cg/M2 stimulation. We counted the number of spikes fired at each current intensity and trial, and calculated the average number of spikes per trial (>40 trials per stimulation current, as previously explained). The threshold cortical stimulation current was defined as the minimal current driving spike discharges in the recorded neuron. The latency was defined as the time from the cortical stimulation up to the beginning of the first evoked spike. The spontaneous activity was defined as the amount of spontaneous spikes per second. We counted the amount of spikes during intertrial intervals after excluding 0.5 s after each cortical stimulus. When possible, gap-free recordings were used to calculate the spontaneous activity.

Ex vivo recordings. Data analysis was performed with ClampFit (Molecular Devices) and Signal 5.04 software (Cambridge Electronic Design). Resting membrane potential was measured at the baseline before the injection of current pulses, and the input resistance was calculated as the slope of the V/I curve with V measured at the steady state of the response to 500 ms, hyperpolarizing current steps ranging from −20 pA to −150 pA. Rheobase was calculated as the minimal amplitude of a current step that resulted in the firing of at least one spike. Action potential (AP) threshold, width, and amplitude were measured only for the first spike elicited at rheobase.

Viral injections

Under deep surgical anesthesia (isoflurane 1 to 2%), each adult mouse was mounted in a stereotaxic frame (Stoelting) with a mouse adaptor and treated with a local anesthetic in the scalp and pressure points (bupivacaine hydrochloride solution, 5% w/v, Durocaine, AstraZeneca, 0.1-0.3 ml). Ophthalmic ointment was applied in both eyes to prevent corneal desiccation. hM4D-mCherry-DIO virus stocks (virus: AAV.8-hsyn-Dio-

hM4D(Gi) mCherry-WPRE-hGPA, Virovek; lot #16-626) or mCherry-DIO control vector stock (AAV.8-hsyn-DIO-mCherry-WPRE-hGPA, Virovek; lot #v61605), were freshly diluted at 1:3 and 1:6 in sterile PBS, respectively. Mice received bilateral intrastriatal injections of 2 μl of virus dilution (0.5 μl/min) in two sites per striatum: 0.8 mm anterior from bregma, 1.5 mm lateral from midline, and 3 mm (first site) and 2.3 mm (second site) ventral from dura according to the atlas of Paxinos and Franklin (2004). After surgery, the analgesic bupivacaine hydrochloride (5 mg/ml) was injected subcutaneously (10 μl/10 g body weight) around the wound. Mice were housed together in groups of 3-5 mice per cage until testing.

Behavioral experiments and pharmacology

hM4D-mCherry-DIO virus injections were performed in DAN-lesioned and age-matched control mice at 2-4 months of age. An additional group of DAN-lesioned mice were injected with the control mCherry-DIO vector. One month later, mice were tested in a battery of behavioral tests (see Fig. 5A) as previously described (Braz et al., 2015). All behavioral tasks were performed during the light phase. All sessions were video recorded through a camera mounted above the arena, and mouse position was determined by automatic video tracking (ANY-maze). All animals were moved from the mouse colony room to a holding room adjacent to the behavioral test room in their home cages at least 1 h before testing. All findings were confirmed in at least two separate cohorts of animals. All mazes and chambers were thoroughly cleaned with 10% ethanol, dried between subjects, and sanitized at the end of the day.

Large open field. Animals were injected with CNO (3 mg/kg) or saline 30 min before testing. The test was repeated 2 weeks after, and treatments were reversed. Horizontal locomotor activity was assessed in a 1.25-m-diameter circular open field during 15 min. The arena was placed in the center of a room homogeneously illuminated at 100 lux. ANY-maze software was used to track body center. We quantified the total distance traveled to assess the horizontal locomotor activity.

Standard open field. Animals were injected with CNO at 3 mg/kg, CNO at 5 mg/kg, or saline, 30 min before testing. Two weeks were allowed between tests. Horizontal locomotor activity was assessed in an open-field arena (40 cm × 40 cm) during 15 min. Total distance traveled and immobility were used to assess motor activity. The arena was placed in the center of a room (2 × 1.8 m) and was homogeneously illuminated at 100 lux.

Marble burying. Animals were injected with CNO (3 mg/kg) or saline 30 min before testing. The test was repeated 2 weeks after, and treatments were reversed. Each mouse was individually transferred into a cage containing 20 marbles homogeneously distributed over a 5 cm bedding during 20 min. Buried marbles were counted every 5 min from video files.

Histology and immunohistochemistry

At the end of *in vivo* electrophysiological and behavioral experiments, mice received a lethal dose of urethane and were transcardially perfused with 10 ml of 0.04% heparin cold saline solution (Sodic Heparin, Duncan Laboratories, 5000 IU/ml) followed by 20 ml of PFA (4%) in 0.1 M PBS. Brains were removed, immersed overnight in the same fixative at 4°C, and stored in 0.1 M PBS containing 30% sucrose at 4°C for 24-72 h. Coronal sections (30-40 μm thick) were obtained throughout the substantia nigra, dorsal striatum, and frontal cortex using a microtome equipped with a freezing stage and stored free-floating in PBS 0.1 M containing 0.1% sodium azide at 4°C until use. Location of the cortical stimulation electrode was assessed by visual examination of the mechanical tissue damage in the coronal sections using a transmitted light microscope at low magnification (Fig. 1B).

Striatal sections were processed for Neurobiotin labeling to identify juxtacellularly labeled cells as previously described (Escande et al., 2016). Free-floating sections were incubated in 0.1 M PBS containing 10% normal goat serum and 0.3% Triton X-100 at room temperature for 2 h and then overnight in 0.1 M PBS, 0.3% Triton X-100, plus FITC-streptavidin (1:500; Sigma-Aldrich) at 4°C. Sections were mounted on glass slides with anti-fading agent Vectashield (Vector Laboratories). High-resolution
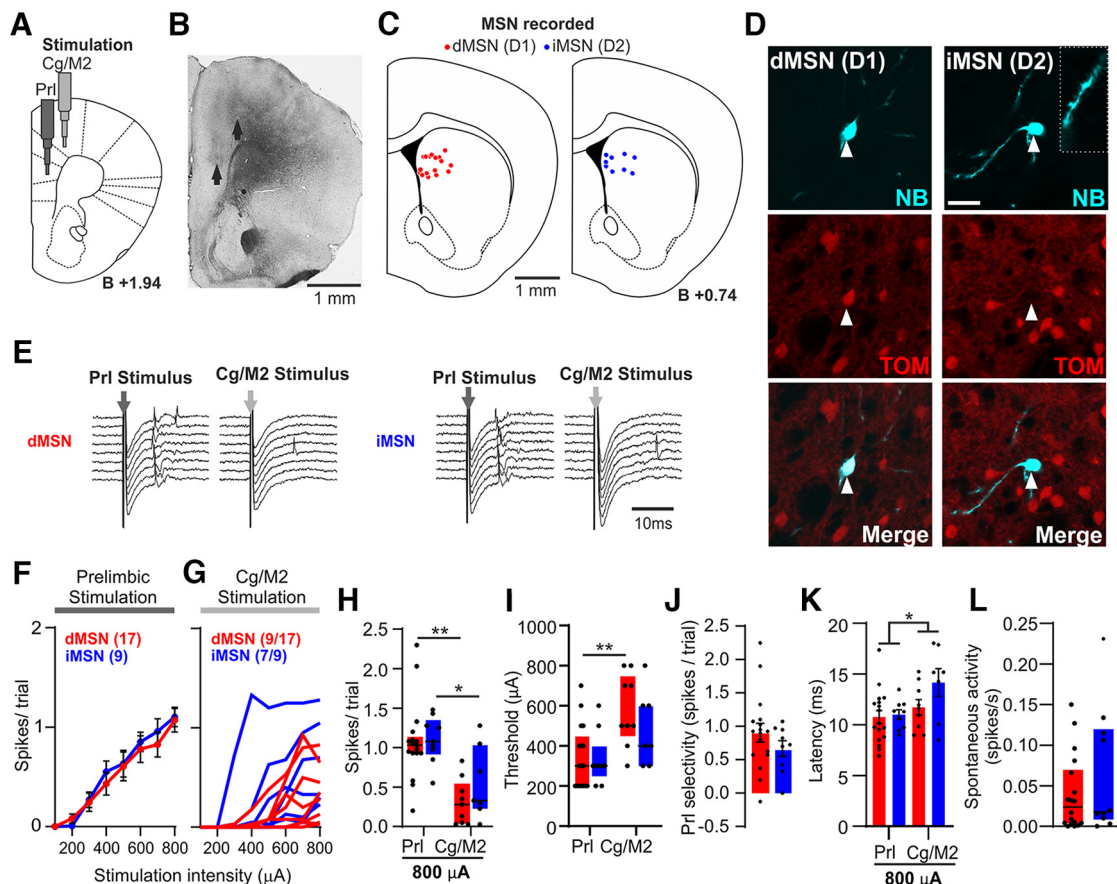
Figure 1. Response of dMSNs and iMSNs to frontal inputs in control animals. ***A***, Schematic diagram of the positioning of Prl and Cg/M2 stimulation electrodes. ***B***, Representative histologic section showing the location of cortical electrodes. ***C***, Reconstruction of the position of the recorded MSN at the site of maximal response for Prl inputs. ***D***, Confocal images of striatal sections showing neurobiotin-filled (NB) neurons (cyan) and tomato (TOM)-positive neurons (red). Left, The neuron was classified as dMSN. Right, The spiny neuron was classified as iMSN (for details, see Escande et al., 2016). ***E***, Representative traces showing the responses to Prl and Cg/M2 stimulation of dMSNs (left) and iMSNs (right) in control mice. ***F, G***, Intensity response curves to Prl (***F***) and Cg/M2 (***G***) stimulation for dMSNs and iMSNs. For Prl, the average cells' response is shown. For Cg/M2, each line is a cell, and the number of responding neurons/recorded neurons is shown. dMSNs and iMSNs respond similarly to Prl stimulation (***F***, two-way repeated-measures ANOVA, nonsignificant interaction: $F_{(7168)} = 0.3913$; $p = 0.9065$). They also respond comparably to Cg/M2 stimulation (***G***, Mann–Whitney test, 800 μA: $p = 0.3593$, 700 μA: $p = 0.2853$, 600 μA: $p = 0.2337$). ***H***, Responses to 800 μA are higher for Prl compared with Cg/M2 stimulation (dMSN: Wilcoxon test, **$p = 0.0078$; iMSN: Wilcoxon test, *$p = 0.0313$). ***I***, Response threshold is lower for Prl compared with Cg/M2 stimulation with a similar but nonsignificant trend for iMSNs (dMSNs: Wilcoxon test, **$p = 0.0078$; iMSNs: Wilcoxon test, $p = 0.2188$). ***J***, Prl input selectivity, calculated as the difference between the Prl and Cg/M2 spike responses, does not differ between dMSN and iMSN (unpaired t test, $p = 0.2647$). ***K***, Latency of responses to Prl and Cg/M2 stimulation. dMSNs showed a longer latency for Cg/M2 than for Prl (mixed-effects analysis, significant effect of cortical region, $F_{(1,14)} = 8.180$, *$p = 0.0126$). ***L***, Spontaneous activity of MSN (Mann–Whitney test, $U = 75.5$, $p = 0.5007$). ***H–L***, Each black dot represents an individual cell. Data are mean ± SEM (***F,J,K***) or median and interquartile range (***H,I,L***).

confocal images were obtained from identified labeled neurons on an Olympus Fluoview 1000 system. Confocal images allowed us to identify MSNs by their morphology and to assign them as belonging to direct or indirect pathways (see Results). Confocal images were assembled in ImageJ, and reconstructions of the position of each neuron were made (see Figs. 1C, 2B, 3B).

The extent of DAN lesion was confirmed by immunohistochemical detection of TH as previously described (Galiñanes et al., 2009). Briefly, sections were washed 3 times in PBS 0.1 M with 0.15% Triton X-100 (PBS-T) and incubated in PBS-T with 0.3% H_2O_2 for 30 min at room temperature to inhibit endogenous peroxidase. Then, sections were washed again and were incubated in blocking solution (5% normal goat serum, 0.3% Triton X-100 in PBS) for 2 h at room temperature. Sections were incubated overnight at 4°C with rabbit anti-TH (1/1000; AB152; Millipore) in blocking buffer. Three rinses in PBS-T were performed before incubating the sections with a biotinylated goat anti-rabbit IgG (Vector Laboratories) at a working dilution of 1:800. The antibody–antigen complex was visualized with an avidin-biotin peroxidase complex (Vector Laboratories).

The extent of hM4D-mCherry-DIO viral infections was assessed by hM4D-mCherry immunohistochemical detection in striatal sections. Briefly, tissue sections were washed 3 times in PBS, incubated in PBS 3%

H_2O_2 for 30 min, washed again 3 times, and incubated in blocking solution (5% normal goat serum and 0.3% Triton X-100 in PBS) at room temperature for 2 h. Then, sections were incubated overnight with rabbit anti-mCherry (1/1500, Abcam, ab167453) in blocking buffer. After 3 rinses in PBS, sections were incubated with a biotinylated goat anti-rabbit IgG (1/500, Vector Labs). The antibody–antigen complex was visualized with an avidin-biotin peroxidase complex.

Experimental design and statistical analyses
For juxtacellular experiments (Figs. 1-3) and whole-cell recordings (Fig. 4), *Drd1a-tdTomato* male and female mice (sex was balanced) with DAN lesion and their control littermates (injected with saline as previously explained) were used.

For juxtacellular recordings, a total of 26 control MSNs (17 dMSNs and 9 iMSNs) were recorded from 17 control animals, belonging to 11 different litters. For the control group, all MSNs were tested for their response to Prl and Cg/M2 stimulation. A total of 23 MSNs were recorded from 12 lesioned animals (12 dMSNs and 11 iMSNs). For the lesioned group, all MSNs were tested for their response to Prl and Cg/M2 stimulation, with the exception of one dMSN and one iMSN that could not be tested for Cg/M2 response. Between 1 and 2 neurons were recorded from each animal in 1 day of experiment.
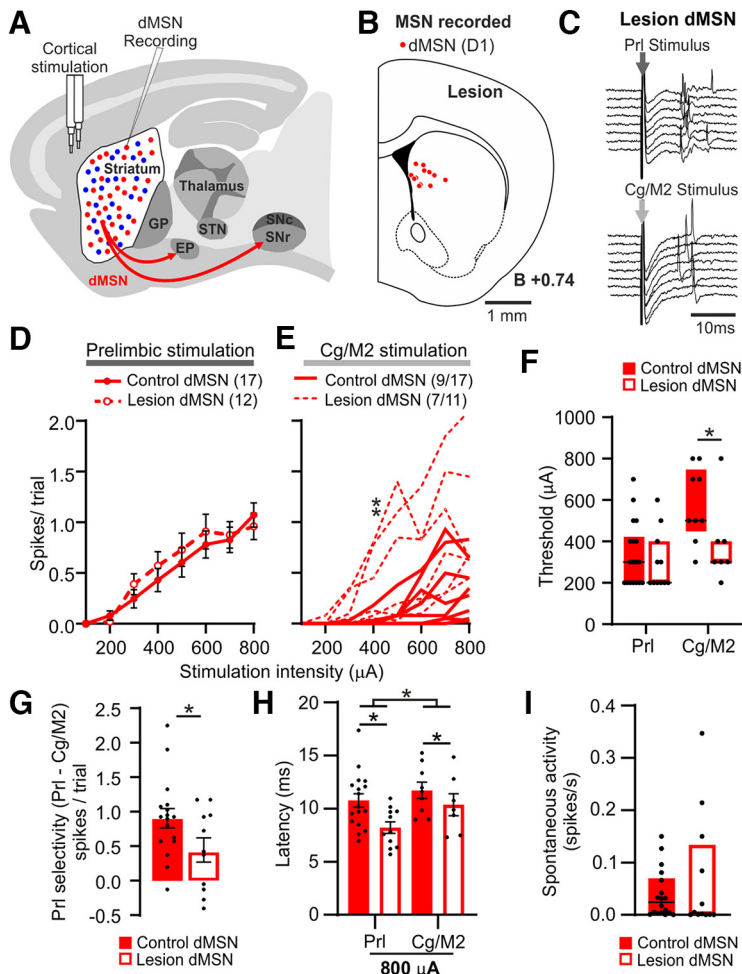
Figure 2. dMSN selectivity is reduced with neonatal dopaminergic lesion. *A*, Schematic representation of the positioning of Prl and Cg stimulation electrodes. *B*, Reconstruction of the position of the recorded dMSNs in lesioned mice. *C*, Representative traces showing responses of dMSN of lesioned animals to Prl and Cg stimulation. *D*, *E*, Intensity response curves of dMSN to Prl (*D*) and Cg (*E*) stimulation. For Prl, the average cells' response is shown. For Cg/M2, each line is a cell, and the number of responding neurons/recorded neurons is shown. There are no differences in the response to Prl stimulation (*D*, two-way repeated-measures ANOVA, nonsignificant interaction: $F_{(7189)} = 0.9441$, $p = 0.4737$). In lesioned animals, dMSNs are more responsive to Cg inputs (*E*, 400 µA: Mann–Whitney test, $U = 50.5$, **$p = 0.0080$). *F*, Minimal cortical stimulation current (threshold) needed to induce dMSN response to Cg/M2 stimulation is lower in lesioned animals (Prl: Mann–Whitney test, $U = 83$, $p = 0.4656$; Cg/M2: Mann–Whitney test, $U = 12.5$, *$p = 0.0398$). *G*, Prl input selectivity, calculated as the difference in Prl and Cg/M2 responses, is reduced in lesioned mice (unpaired *t* test: $t_{(26)} = 2.064$, *$p = 0.0492$). *H*, Latency of dMSN response to Prl and Cg/M2 stimulation is shorter in lesioned animals, and latencies are longer for Cg/M2 than for Prl (mixed-effects analysis: significant effect of lesion, $F_{(1,27)} = 6.439$, *$p = 0.0173$; significant effect of cortical region, $F_{(1,13)} = 4.982$, *$p = 0.0438$). *I*, Spontaneous activity of dMSN did not differ between groups (Mann–Whitney test, $U = 95$, $p = 0.5936$). *F–I*, Each black dot represents an individual cell. Data are mean ± SEM (*G,H*) or median and interquartile range (*F,I*).

For whole-cell recordings of MSN (Fig. 4), we recorded a total of 14 control MSNs (7 dMSNs and 7 iMSNs) coming from 5 control animals, and 18 neurons from 5 lesioned animals (9 dMSNs and 7 iMSNs), belonging to 5 different litters, including animals of both sexes.

For behavioral experiments, we used D1-Cre-positive male and female mice (resultant from *D1-Cre* × WT mattings, sex was balanced) with neonatal lesion and hM4D-mCherry-DIO virus injection. A total of 18 animals were used belonging from 9 different litters.

Data were organized using Microsoft Excel and GraphPad 8, and statistical analyses were made using SigmaPlot 11.0 and GraphPad 8. Data are presented as mean ± SEM or median with interquartile range. For comparisons involving two groups, we used an unpaired *t* test or Mann–Whitney test (or paired *t* test or Wilcoxon matched-pairs signed rank test when appropriate). If two factors were present, a two-way ANOVA

or two-way repeated measures ANOVA followed by Tukey's or Sidak's comparisons was used, as described in the figure legends. For the analysis of response latencies to Prl and Cg/M2 stimulation, since some neurons did not respond to Cg/M2 input and then the number of observations for each input was different, a mixed-effects analysis was used.

Results

In vivo DMS-MSN response to frontal inputs

In a previous study (Braz et al., 2015), we used an electrode array and local field potential recordings to map cortical inputs to the dorsal striatum *in vivo* and found a topographical organization where the DMS receives a strong input from the Prl cortex and less marked convergent inputs from more lateral frontal cortical areas, such as the Cg/M2 cortex (Van De Werd and Uylings, 2014). This mapping of corticostriatal inputs is in agreement with anatomic findings (Voorn et al., 2004; Wall et al., 2013; Hintiryan et al., 2016), but detailed functional *in vivo* studies at the level of individual DMS-dMSNs and iMSNs were lacking. To study the *in vivo* response of dMSNs and iMSNs to frontal cortex stimulation (Fig. 1A–C), we performed blind juxtacellular recordings in urethane-anesthetized adult *Drd1a-tdTomato* transgenic mice, using previously published methods (Escande et al., 2016). Because MSNs fire spontaneously at very low rates, they were detected by evoking orthodromic responses to cortical stimulation at high-stimulation intensities while the recording electrode descended through the striatum. After isolating a single unit, the spike response to electrical stimulation of the Prl and Cg/M2 cortices at increasing current intensities was determined. Postmortem, the neurobiotin-filled spiny neurons were classified as dMSNs if they expressed tomato or as iMSNs if they did not (Fig. 1D) (for details, see Escande et al., 2016).

Intensity–response curves to Prl stimulation showed similar spike discharge responses of dMSNs and iMSNs (Fig. 1E,F, two-way repeated-measures ANOVA, nonsignificant interaction: $F_{(7168)} = 0.3913$; $p = 0.9065$). At current intensities of stimulation >700 µA, both types of MSN responded to every Prl stimulation trial without failure (Fig. 1F). In contrast, at these current intensities, 9 of 17 dMSNs and 7 of 9 iMSNs responded to Cg/M2 stimulation trials (Fig. 1E,G). The proportion of cells that responded to both inputs did not differ between MSN types (Fisher's exact test, $p = 0.3989$). Moreover, both types of MSNs showed more marked responses to Prl input than Cg/M2 input at high-stimulation current intensity (Fig. 1H; dMSNs: Wilcoxon test, $p = 0.0078$; iMSNs: Wilcoxon test, $p = 0.0313$). Accordingly, less current was required to evoke a response (threshold current) in dMSNs by stimulating the Prl than Cg/M2, with a similar but nonsignificant tendency for iMSNs (Fig. 1I; dMSNs: Wilcoxon test, $p = 0.0078$; iMSNs: Wilcoxon test, $p = 0.2188$). Response selectivity to Prl stimulation, calculated as the difference between the spike discharge responses to Prl and Cg/M2 stimulation at

maximal stimulation current intensity, did not differ between MSN types (Fig. 1*J*; unpaired *t* test, $t_{(24)} = 1.142$, $p = 0.2647$). dMSN and iMSN responses to Cg/M2 input showed a longer latency than responses to Prl input (Fig. 1*K*, mixed-effects analysis, significant effect of cortical region, $F_{(1,14)} = 8.180$, $p = 0.0126$). Finally, both cell types exhibited similar levels of spontaneous activity (Fig. 1*L*, Mann–Whitney test, $U = 0.5007$, $p = 0.5007$).

Overall, the data show that the Prl provides equally strong functional inputs to both populations of DMS-MSNs and that both types of MSNs show more marked responses to Prl than Cg/M2 inputs.

Dopamine availability during postnatal development differentially affects frontal input to dMSN and iMSN

Our previous local field potential studies showed that early induction of dopamine depletion distorts the topographical representation of cortical inputs into the dorsal striatum (Braz et al., 2015); however, it is not clear whether early dopamine availability differentially affects dMSN and iMSN Prl selectivity. Therefore, we analyzed the dMSN and iMSN *in vivo* response to Prl and Cg/M2 stimulation (Figs. 2*A–C*, 3*A–C*) in adult animals that have suffered a neonatal DAN lesion (Galiñanes et al., 2009; Braz et al., 2015).

The proportion of cells that responded to both inputs was not affected by the lesion (lesion dMSNs: 64%, 7 of 11 neurons; control dMSNs: 53%, 9 of 17 neurons; Fisher's exact test, $p = 0.7047$; lesion iMSNs: 60%, 6 of 10 neurons; control iMSNs: 78%, 7 of 9 neurons; Fisher's exact test, $p = 0.6285$). Moreover, the dopaminergic lesion did not affect the response of dMSNs to Prl stimulation (Fig. 2*D*, two-way repeated-measures ANOVA, nonsignificant interaction: $F_{(7189)} = 0.9441$, $p = 0.4737$). The dMSN response to Cg/M2 stimulation showed a high variability (Fig. 2*E*) with an increased magnitude at 400 µA in lesioned animals (Mann–Whitney test, $U = 8.5$, $p = 0.008$). Moreover, the Cg/M2 threshold stimulation current required to evoke spikes was decreased for dMSN in lesioned animals (Fig. 2*F*, Prl: Mann–Whitney test, $U = 83$, $p = 0.4656$; Cg/M2: Mann–Whitney test, $U = 12.5$, $p = 0.0398$), suggesting that the dMSN response to Cg/M2 input was increased by the lesion. Consistently, response selectivity to Prl stimulation was lower in dMSN of lesioned animals (Fig. 2*G*; unpaired *t* test: $t_{(26)} = 2.064$, $p = 0.0492$). The latency of Prl and Cg/M2 responses in dMSNs was shorter in DAN-lesioned animals (Fig. 2*H*; mixed-effects analysis: significant effect of lesion, $F_{(1,27)} = 6.439$, $p = 0.0173$; significant effect of cortical region, $F_{(1,13)} = 4.982$, $p = 0.0438$), whereas the spontaneous activity of
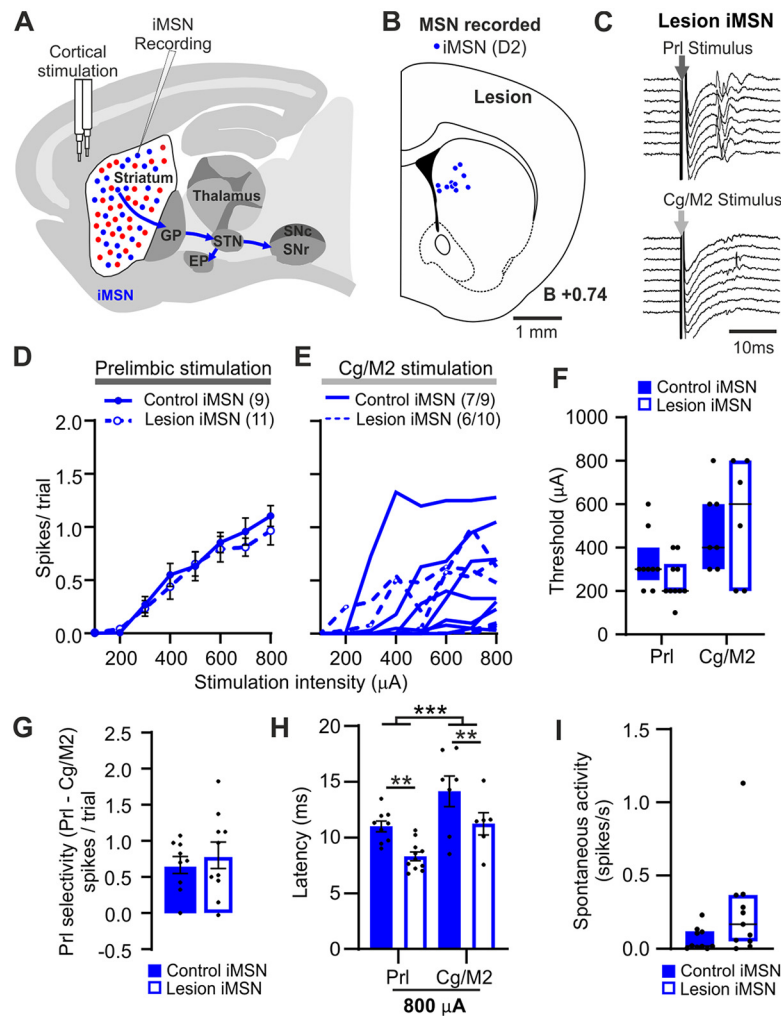

Figure 3. Response of iMSNs to frontal inputs after neonatal dopaminergic lesion. **A**, Schematic representation of the positioning of Prl and Cg stimulation electrodes. **B**, Reconstruction of the position of the recorded iMSNs in lesioned mice. **C**, Representative traces showing responses of iMSN of lesioned animals to Prl and Cg stimulation. **D**, **E**, Intensity response curves to Prl (**D**) and Cg/M2 (**E**) stimulation for iMSNs. For Prl, the average cells' response is shown. For Cg/M2, each line is a cell, and the number of neurons with response/total neurons is shown. There are no differences in the response to Prl (two-way repeated-measures ANOVA, nonsignificant interaction: $F_{(7126)} = 0.5534$, $p = 0.7923$) and Cg/M2 stimulation between treatments (Mann–Whitney test, 800 µA: $p = 0.4685$, 700 µA: $p = 0.3456$, 600 µA: $p = 0.5542$). **F**, There are no differences in iMSN response threshold between treatments (Prl: Mann–Whitney test, $p = 0.1420$; Cg/M2: Mann–Whitney test, $p = 0.8089$). **G**, There is no difference in Prl input selectivity defined as difference between Prl and Cg response (unpaired *t* test, $t_{(17)} = 0.6090$, $p = 0.5506$). **H**, Latency of iMSN response to Prl and Cg/M2 stimulation was shorter in lesioned animals, and latencies are longer for Cg/M2 than for Prl (mixed-effects analysis: significant effect of lesion, $F_{(1,18)} = 9.064$, **$p = 0.0075$; significant effect of cortical region, $F_{(1,11)} = 20.96$, ***$p = 0.0008$). **I**, Spontaneous activity of iMSNs did not differ between groups (Mann–Whitney test, $U = 28.5$, $p = 0.0623$). **F–I**, Each black dot represents an individual cell. Data are mean ± SEM (**G,H**) or median and interquartile range (**F,I**).

dMSNs was not affected by the lesion (Fig. 2*I*, Mann–Whitney test, $U = 95$, $p = 0.5936$).

In contrast, the response of iMSN to either Prl stimulation or Cg/M2 stimulation, as assessed in intensity–response curves (Fig. 3*D*, two-way repeated-measures ANOVA, nonsignificant interaction: $F_{(7,126)} = 0.5534$, $p = 0.7923$; Fig. 3*E*, nonsignificant Mann–Whitney test), or cortical stimulation threshold currents (Fig. 3*F*, Prl: Mann–Whitney test, $U = 28$, $p = 0.1420$; Cg/M2: Mann–Whitney test, $U = 19$, $p = 0.8089$), and therefore, their Prl selectivity (Fig. 3*G*: unpaired *t* test, $t_{(17)} = 0.6090$, $p = 0.5506$) remained unchanged, suggesting that early dopamine depletion has a more marked impact on dMSN than iMSN function. The latency of Prl and Cg/M2 responses in iMSN was shorter in
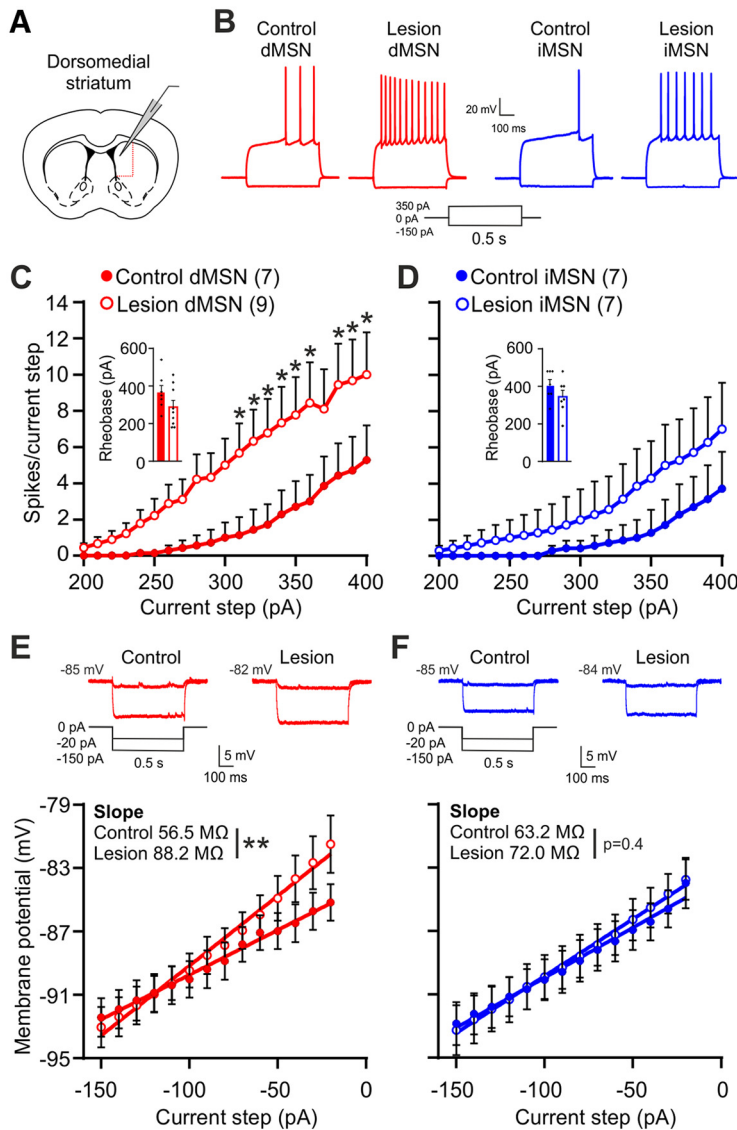
Figure 4. Intrinsic excitability of dMSNs is increased after neonatal dopaminergic lesion. **A,** We performed whole-cell recordings in brain slices to study the excitability of dMSNs and iMSNs in *Drd1a-tdTomato* mice with neonatal dopaminergic depletion and their control littermates. **B,** Representative traces of neuronal responses to 0.5 s current steps of −150 and 350 pA for dMSNs (red traces) and iMSNs (blue traces). **C, D,** Spike counting for each current step for dMSNs (**C**) and iMSNs (**D**). In lesioned animals, dMSNs (**C**) are more excitable (two-way repeated-measures ANOVA, significant interaction: $F_{(20,280)} = 2.239$, $p = 0.0021$; *$p < 0.05$ Tukey comparisons) with no differences for iMSNs (**D**, two-way repeated-measures ANOVA, nonsignificant interaction: $F_{(20,240)} = 0.8561$, $p = 0.6431$). Insets, Rheobase current (**C**, unpaired t test, $t_{(14)} = 1.510$, $p = 0.1534$; **D**, unpaired t test, $t_{(12)} = 1.368$, $p = 0.1965$). **E, F,** Membrane potential responses to hyperpolarizing current steps. Representative traces of neuronal responses to 0.5 s current steps of −20 and −150 pA for dMSNs and iMSNs are shown. The slope of the curve (input resistance) is higher for dMNS (**E**) in lesion animals (linear regression, difference between slopes is significant, $F_{(1,220)} = 7.696$, **$p < 0.01$ with no changes for iMSNs (**F**, linear regression, $F_{(1,196)} = 0.5470$, $p = 0.4605$).

DAN-lesioned animals (Fig. 3H; mixed-effects analysis: significant effect of lesion, $F_{(1,18)} = 9.064$, $p = 0.0075$; significant effect of cortical region, $F_{(1,11)} = 20.96$, $p = 0.0008$), whereas the spontaneous activity of iMSN was not affected by the lesion (Fig. 3I; Mann–Whitney test, $U = 28.5$, $p = 0.0623$).

Together, our data show that in the absence of dopamine regulation since early postnatal development, both types of adult DMS-MSNs show preserved responses to PrI stimulation with a shorter latency. Moreover, DMS-dMSN become more responsive to Cg/M2 inputs and therefore less PrI selective.

Intrinsic excitability of dMSN increases after neonatal dopaminergic lesion

A recent study in a genetic model in which a mutation of the PITX3 gene leads to a developmental loss of the dopaminergic innervation of the striatum showed that dMSN excitability is very high early after birth and does not descend to adult levels during the first postnatal weeks because of a diminished dopamine-dependent maturation of a potassium inwardly rectifying current (Kir) (Lieberman et al., 2018). Moreover, in a previous study, we found that dMSNs and iMSNs show a shrunken dendritic arbor in neonatally DAN-lesioned animals, which could result in a higher input resistance (Braz et al., 2015). Because a higher intrinsic excitability could explain why adult dMSNs remain responsive to cortical input despite the neonatal dopaminergic lesion, we performed *ex vivo* whole-cell recordings to study the response of dMSNs and iMSNs to somatic current injection in *Drd1a-tdTomato* mice with neonatal dopaminergic depletion and *Drd1a-tdTomato* sham-lesioned mice (Fig. 4A,B). Interestingly, dMSNs in lesioned mice showed a higher spiking response to depolarizing steps of current injection (Fig. 4C, two-way repeated-measures ANOVA, significant interaction: $F_{(20,280)} = 2.239$, $p = 0.0021$; Tukey comparisons, control vs lesion $p < 0.05$ from 310-400 pA), and a similar but nonsignificant trend was observed in iMSNs (Fig. 4D, two-way repeated-measures ANOVA, nonsignificant interaction: $F_{(20,240)} = 0.8561$, $p = 0.6431$). There was no difference in the rheobase current (Fig. 4C, inset: unpaired t test, $t_{(14)} = 1.510$, $p = 0.1534$; Fig. 4D, inset: unpaired t test, $t_{(12)} = 1.368$, $p = 0.1965$). Input resistance (Rin) was assessed by fitting a line to the membrane potential responses to hyperpolarizing current steps that drove the membrane potential to values near the potassium equilibrium potential, where the Kir current has a strong influence in MSNs (Gertler et al., 2008). A steepest slope of the curve indicative of a higher Rin was observed in the dMSNs of neonatally lesioned animals (Fig. 4E, linear regression, differences between slopes are significant, $F_{(1220)} = 7.696$, $p < 0.001$), with no changes of Rin in iMSNs (Fig. 4F, $F_{(1192)} = 0.470$, $p = 0.4605$). The resting membrane potential and the AP amplitude and duration were not affected by the lesion (Table 1).

Overall, our results show that low dopamine levels during postnatal development result in a higher intrinsic excitability of adult DMS-dMSNs.

The stimulatory tone of dMSN on locomotion is preserved despite neonatal dopaminergic lesion

In animals rendered parkinsonian by lesioning midbrain DANs during adulthood, DMS-dMSNs are markedly hypoactive (Parker et al., 2018; Ryan et al., 2018) and optogenetic activation of DMS-dMSNs rescues locomotor activity (Kravitz et al., 2010). By contrast, the present data show that dMSNs are hyperexcitable and fully responsive to cortical input in animals with neonatal dopaminergic

Table 1. Electrophysiological properties of dMSN and iMSN in control and lesion conditions[a]

Parameter (mean ± SEM)		Resting potential (mV)	AP amplitude (mV)	AP duration (ms)
dMSN	Control	−84 ± 1	77 ± 2	1.01 ± 0.05
	Lesion	−79 ± 2	74 ± 3	1.20 ± 0.07
Statistics	$t_{(df)}$	$t_{(14)} = 1.606$	$t_{(14)} = 0.7585$	$t_{(14)} = 1.930$
	p value	0.1305	0.4607	0.0741
iMSN	Control	−83 ± 1	73 ± 5	1.07 ± 0.07
	Lesion	−82 ± 1	74 ± 4	1.14 ± 0.03
Statistics	$t_{(df)}$	$t_{(12)} = 0.5635$	$t_{(12)} = 0.1620$	$t_{(12)} = 0.8903$
	p value	0.5835	0.874	0.3908

[a]The resting membrane potential, and the AP amplitude and duration were not affected by the lesion. Data are mean ± SEM.

lesion. Therefore, we asked whether preserved locomotion in neonatally lesioned mice depends on dMSN activity tone. With this aim, we performed a chemogenetic inhibition of DMS-dMSNs in lesioned animals and their control littermates, and we analyzed its effect on locomotion (Fig. 5A). We performed neonatal dopaminergic lesions in Drd1a-Cre mice pups; and in adulthood, we injected a virus that expresses, in a Cre recombinase-dependent manner, a modified M4 muscarinic receptor (hM4D(Gi)-mCherry-DIO) that induces inhibition in response to CNO (Roth, 2016). Previous studies have shown that neonatal DAN loss effects on locomotion and exploration are context-dependent and that these animals show normal anxiety levels (Braz et al., 2015); locomotion is preserved in large arenas inducing high levels of exploratory activity in control animals and can be increased in standard arenas under conditions that raise lower levels of exploration in control animals (Avale et al., 2004a; Galiñanes et al., 2009; Braz et al., 2015). Therefore, we assessed locomotion in a large size open field that promotes high levels of locomotion and in a standard size open field (Braz et al., 2015). The animals were treated with saline or CNO in different test sessions separated by at least a week (Fig. 5A). After the behavioral experiments, we confirmed the expression of hM4D-mCherry (Fig. 5B) in the DMS and the extent of the lesion (Fig. 5C) by means of postmortem histology, and the effect of CNO administration on dMSN somatic excitability by performing *ex vivo* whole-cell recordings (Fig. 5D). CNO application decreased the spiking response to depolarizing current steps (Fig. 5E: two-way repeated-measures ANOVA, significant interaction: $F_{(40,160)} = 2.765$, $p < 0.0001$, Sidak's comparisons, with vs without CNO, $p < 0.05$ from 340 to 400 pA; Fig. 5F: two-way repeated-measures ANOVA, significant interaction: $F_{(40,320)} = 4.879$, $p < 0.0001$; Sidak's comparisons, with vs without CNO, $p < 0.05$ from 270 to 400 pA) and increased the rheobase current (Fig. 5G, two-way repeated-measures ANOVA, significant effect of CNO application: $F_{(1,6)} = 27.14$, $p = 0.002$) of mCherry-positive dMSN, overall decreasing their excitability.

In the large open field, CNO administration (3 mg/kg, i.p., latin square design) reduced the distance traveled (Fig. 6A: two-way repeated-measures ANOVA, significant effect of CNO: $F_{(1,15)} = 46.27$, $p < 0.0001$; Fig. 6B: unpaired t test, $t_{(15)} = 1.096$, $p = 0.2902$; Fig. 6C: unpaired t test: $t_{(15)} = 1.190$, $p = 0.2524$) and increased the time immobile (Fig. 6D: two-way repeated-measures ANOVA, significant interaction: $F_{(1,15)} = 7.957$, $p = 0.0129$; Holm–Sidak comparisons: control, saline vs CNO, $p < 0.01$; lesion, saline vs CNO, $p < 0.001$), both in lesioned and control mice. This is consistent with the general view that dMSN activity promotes locomotion (Albin et al., 1989) and supports the hypothesis that dMSN activity is necessary to preserve locomotion after the neonatal dopaminergic lesion. Strikingly, the effect of

CNO on the immobility time was higher in lesioned mice (Fig. 6E: unpaired t test, $t_{(15)} = 2.821$, $p = 0.0129$; Fig. 6F: Mann–Whitney test, $U = 13$, $p = 0.0274$), suggesting that the dependence of general motility on the stimulatory tone of dMSNs increases after neonatal dopaminergic lesion. A similar result was obtained in a standard size open field (Fig. 6G,H). CNO treatment (3 and 5 mg/kg, i.p.) reduced the total distance traveled (Fig. 6G, two-way repeated-measures ANOVA, effect of CNO: $F_{(2,16)} = 7.702$, $p = 0.0045$; Holm–Sidak's comparisons in lesioned animals: saline vs CNO 3 mg/kg, $p < 0.05$; saline vs CNO 5 mg/kg, $p < 0.01$) and increased the time immobile (Fig. 6H, two-way repeated-measures ANOVA, effect of CNO: $F_{(2,16)} = 6.930$, $p = 0.0068$; Holm–Sidak's comparisons in lesioned animals: saline vs CNO 3 mg/kg, $p < 0.05$; saline vs CNO 5 mg/kg, $p < 0.01$). In contrast, CNO had no effect in a group of lesioned animals transfected with a control vector expressing mCherry but not hM4D, neither in the large open field (Fig. 6I, distance traveled, paired t test, $t_{(5)} = 0.2523$, $p = 0.8109$; time immobile, paired t test, $t_{(5)} = 0.8733$, $p = 0.4225$) nor in the standard open field (Fig. 6J, distance traveled, one-way repeated-measures ANOVA, $F_{(2,10)} = 3.803$, $p = 0.0591$; time immobile, one-way repeated-measures ANOVA $F_{(2,10)} = 2.904$, $p = 0.1013$). Importantly, as shown in previous studies (Braz et al., 2015), neonatal DAN lesion animals also showed marked behavioral alterations in the marble burying test (Fig. 6K) despite the preserved locomotor activity, which were not mitigated by the chemogenetic treatment (Fig. 6L, two-way repeated-measures ANOVA, nonsignificant effect of the lesion: $F_{(1,14)} = 4.245$, $p = 0.0585$; Fig. 6M, two-way repeated-measures ANOVA, significant effect of the lesion, $F_{(1,14)} = 8.184$, $p = 0.0126$; Sidak's comparisons, control vs lesion $p < 0.01$ at $t = 10$ min, $p < 0.05$ at $t = 15$ min; Fig. 6N, two-way repeated-measures ANOVA, effect of the lesion, $F_{(1,14)} = 5.439$, $p = 0.0351$). CNO had no effect in the marble burying test in a group of lesioned mice transfected with the mCherry control vector (Fig. 6O, two-way repeated-measures ANOVA, nonsignificant effect of CNO, $F_{(1,5)} = 0.0002465$, $p = 0.9881$).

Discussion

The mechanisms of the age-dependent effects of striatal dopamine depletion on locomotor activity remain poorly understood. In physiological conditions, locomotion depends on dMSN activity as demonstrated by studies that have assessed the effect of selectively ablating or inhibiting dMSN activity on locomotion (Durieux et al., 2009; Kravitz et al., 2010; Alcacer et al., 2017) and have stressed the relationship between dMSN activity and movement speed (Yttri and Dudman, 2016; Parker et al., 2018; Fobbs et al., 2020). Moreover, dMSNs are almost unresponsive to motor cortex stimulation (Escande et al., 2016), severely depleted of dendritic spines (Suárez et al., 2014; Gomez et al., 2019), and markedly hypoactive (Parker et al., 2018; Ryan et al., 2018) in animals rendered parkinsonian by inducing nigrostriatal degeneration in adulthood. On the other hand, increasing dMSN activity restores locomotion in this condition (Kravitz et al., 2010; Alcacer et al., 2017). The present data show that dMSNs are fully responsive to cortical input in the DMS, which is the most severely denervated striatal region in the neonatal nigrostriatal lesion model (Galiñanes et al., 2009; Braz et al., 2015). Together with our data showing that selective chemogenetic inhibition of DMS-dMSN in adulthood reduces locomotion in the neonatally lesioned animals to a similar or greater extent than in control animals, these findings support that developmental mechanisms
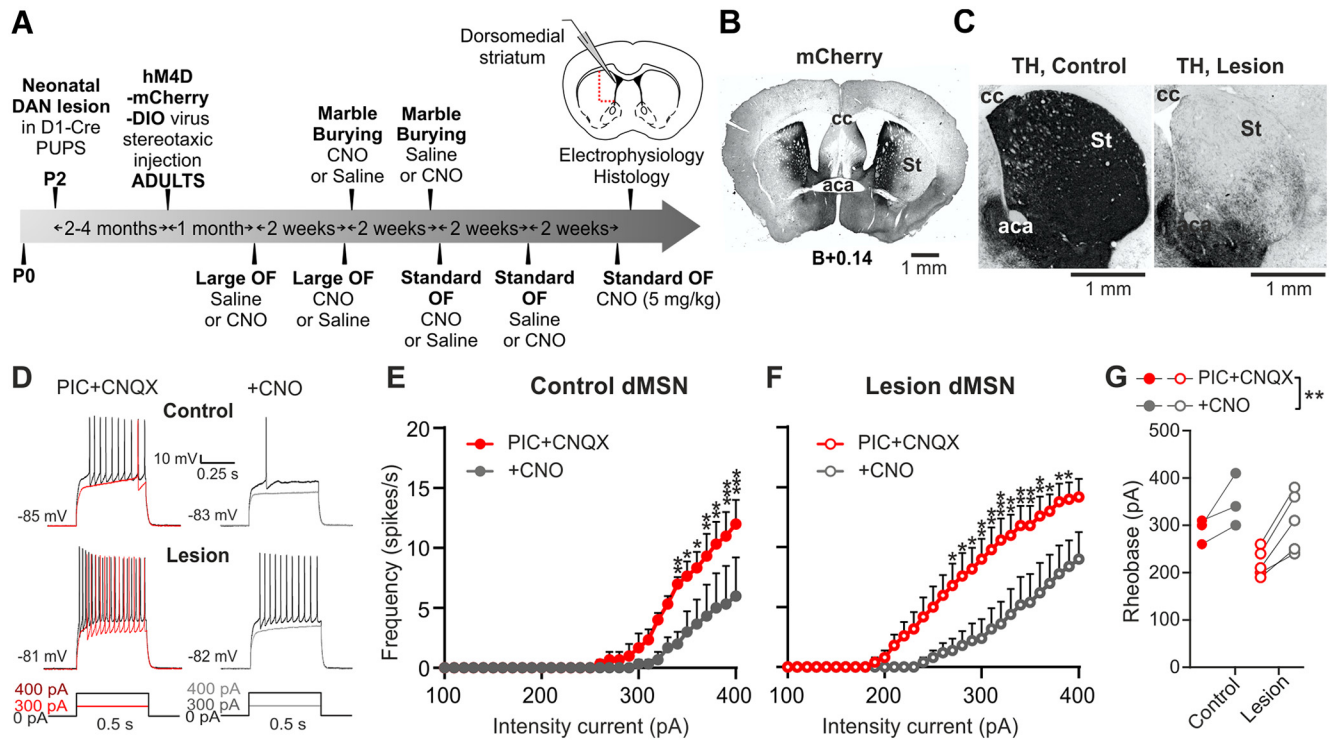
Figure 5. Experimental approach to analyze the chemogenetic inhibition of dMSN on locomotion. **A**, DAN lesion was performed in *D1-Cre* pups at P2 and at 2-4 months of age they received intrastriatal injections of hM4D-mCherry-DIO or mCherry-DIO virus. At least 4 weeks after surgery, animals received intraperitoneal injections of saline or CNO (3 mg/kg) and 30 min after they were tested in a large open field (OF). After 2 weeks, the same animals were tested again and treatments were inverted. A similar scheme was used for the marble burying test (3 mg/kg) and the standard OF (3 and 5 mg/kg). After the behavioral experiments, we performed *ex vivo* whole-cell recordings to confirm the effect of CNO administration on the somatic excitability of mCherry-positive dMSNs. Histologic analyses were performed on coronal brain sections. **B**, Histologic section showing the immunostaining detection of mCherry. St, Striatum; aca, anterior commissure; cc, corpus callosum. **C**, The extent of DA denervation was examined by performing TH immunostaining. **D**, Representative traces of neuronal responses to 0.5 s current steps of 300 and 400 pA for dMSNs before (picrotoxin [PIC] + CNQX) and after CNO application (+CNO). **E**, **F**, CNO application decreases the spiking response to depolarizing current steps in control (**E**, two-way repeated-measures ANOVA, significant interaction: $F_{(40,160)} = 2.765$, $p < 0.0001$; *$p < 0.05$, **$p < 0.01$, ***$p < 0.001$ Sidak's comparisons) and lesioned animals (**F**, two-way repeated-measures ANOVA, significant interaction: $F_{(40,320)} = 4.879$, $p < 0.0001$; *$p < 0.05$, **$p < 0.01$, ***$p < 0.001$ Sidak's comparisons). **G**, CNO application increases the rheobase current in dMSN (two-way repeated-measures ANOVA, significant effect of CNO application: $F_{(1,6)} = 27.14$, **$p = 0.002$).

not available in the mature brain have lasting effects that preserve dMSN tone on locomotion.

When the degeneration of nigrostriatal DANs is induced in the adult, dMSNs show an increase in membrane excitability (Fieblinger et al., 2014a; Suárez et al., 2014; Graves and Surmeier, 2019) as a likely homeostatic response (Fieblinger et al., 2014b) that results insufficient to maintain their basal and evoked activity *in vivo* (Escande et al., 2016; Parker et al., 2018; Ryan et al., 2018). The neonatal lesion model also shows an increase of membrane excitability, which together with the normal spine density observed in this animal model in previous studies (Braz et al., 2015), may suffice to preserve the response of dMSNs to cortical input and their drive on locomotion, as evidenced by the inhibitory effect on locomotor activity of a chemogenetically induced decrease of dMSN membrane excitability. A recent study has shown that the high membrane excitability normally displayed by dMSNs early after birth decreases markedly before puberty because of dopamine effects that promote the functional expression of an inward rectifier potassium (Kir) current (Lieberman et al., 2018). This current experiences a marked postnatal increase in MSN (Cepeda et al., 1991; Tepper et al., 1998), and mice developmentally deficient of striatal dopamine show a reduced postnatal development of this current in dMSNs (Lieberman et al., 2018). Maturation of the Kir current allows the emergence of the distinctive membrane potential alternation between up and down states first observed in rodent MSN during the third postnatal week (Tepper et al.,

1998). At this point, the Kir current becomes sufficient to override the effects of AMPAR and NMDAR stimulation when afferent activity is weak, but not when it is strong, promoting fast transitions to and from down states (Wilson, 1993; Plenz and Kitai, 1998; Tseng et al., 2007; Pomata et al., 2008). Although we have not directly assessed the Kir current, a reduction of this current could contribute to the increase of input resistance we observed at membrane potentials similar to those reached during physiological down states. In addition, shrinkage of the dendritic arbor, a feature previously observed in MSNs of mice developmentally depleted of nigrostriatal DANs (Braz et al., 2015; Suarez et al., 2018), may also contribute to the increased input resistance. In turn, an increase of intrinsic excitability is a likely explanation for both the preservation and shorter latency of dMSN response to cortical inputs despite the dopamine loss, and for their higher response to nonpreferred Cg/M2 inputs and the consequent loss of input selectivity. Further studies are needed to determine whether changes in synaptic strength also contribute to these findings.

Interestingly, modulating MSN activity during a short prepubertal period has lasting effects on MSN spine density in mice (Kozorovitskiy et al., 2012). Indeed, Kozorovitskiy et al. (2012) have shown that selectively inhibiting dMSN activity reduces the formation of dendritic spines in MSN through effects likely mediated by reduced activity in BG-thalamo-cortical loops and reduced glutamate release by corticostriatal afferents, while increasing corticostriatal activity increases spine density in MSN.
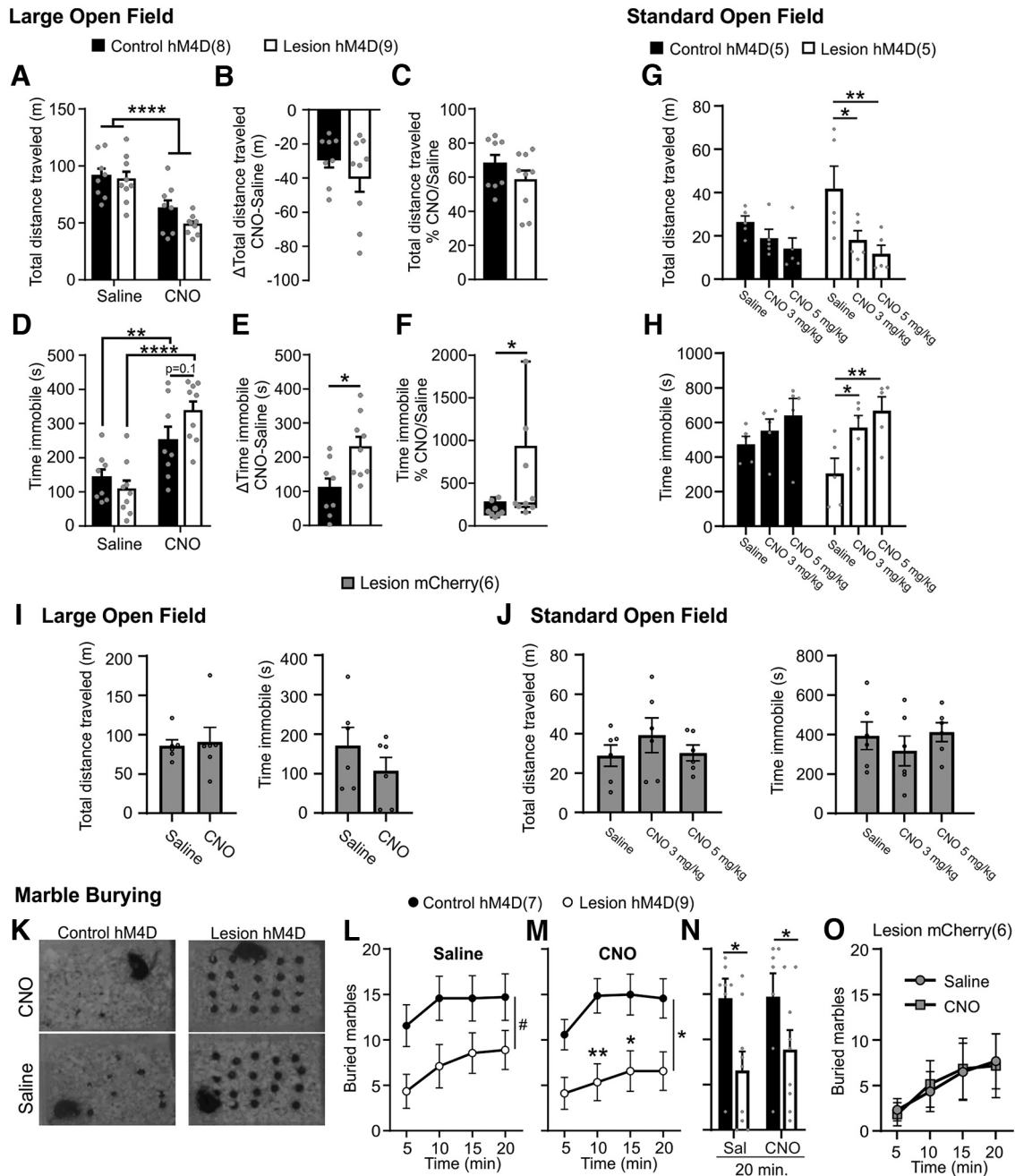
Figure 6. Neonatal dopaminergic lesion increases the stimulatory tone of dMSNs on locomotion. **A**, Total distance traveled in a large open field is reduced by CNO 3 mg/kg (two-way repeated-measures ANOVA, significant effect of CNO: $F_{(1,15)} = 46.27$, ****$p < 0.0001$). **B, C**, The difference (**B**) and the ratio (**C**) between the distance traveled in CNO and Saline condition is not changed between sham and lesioned mice (**B**: unpaired t test, $t_{(15)} = 1.096$, $p = 0.2902$; **C**: unpaired t test: $t_{(15)} = 1.190$, $p = 0.2524$). **D**, The immobility time is increased with CNO treatment (repeated-measures ANOVA, significant interaction: $F_{(1,15)} = 7.957$, $p = 0.0129$; **$p < 0.005$, ****$p < 0.0001$ Holm–Sidak post hoc comparisons). **E, F**, The difference (**E**) and the ratio (**F**) between the time immobile in CNO and Saline condition is greater for lesioned mice (**E**: unpaired t test, $t_{(15)} = 2.821$, *$p = 0.0129$; **F**: Mann–Whitney test, $U = 13$, *$p = 0.0274$). **G, H**, In a standard open field, CNO treatment (3 mg/kg and 5 mg/kg) in lesioned animals reduces the total distance traveled (**G**, two-way repeated-measures ANOVA, effect of CNO: $F_{(2,16)} = 7.702$, $p = 0.0045$; *$p < 0.05$, **$p < 0.01$ Holm–Sidak's comparisons) and increases the time immobile (**H**, two-way repeated-measures ANOVA, effect of CNO: $F_{(2,16)} = 6.930$, $p = 0.0068$; *$p < 0.05$, **$p < 0.01$ Holm–Sidak's comparisons). **I, J**, CNO had no effect in a group of lesioned animals transfected with a control vector without hM4D (mCherry vector), neither in the large open field (3 mg/kg, **I**: distance traveled, paired t test, $t_{(5)} = 0.2523$, $p = 0.8109$; time immobile, paired t test, $t_{(5)} = 0.8733$, $p = 0.4225$), nor in the standard open field (3 and 5 mg/kg, **J**: distance traveled, one-way repeated-measures ANOVA, $F_{(2,10)} = 3.803$, $p = 0.0591$; time immobile, one-way repeated-measures ANOVA $F_{(2,10)} = 2.904$, $p = 0.1013$). **K**, Representative images of the marble burying test at 20 min. **L, M**, Lesioned animals bury less marbles (**L**: two-way repeated-measures ANOVA, treatment factor effect: $F_{(1,14)} = 4.245$, #$p = 0.0585$), and their performance is not improved by CNO 3 mg/kg treatment (**M**: two-way repeated-measures ANOVA, treatment factor effect: $F_{(1,14)} = 8.184$, *$p = 0.0126$; **$p < 0.01$, *$p < 0.05$ Sidak's comparisons). **N**, Buried marbles after 20 min of the test (two-way repeated-measures ANOVA, effect of the lesion, $F_{(1,14)} = 5.439$, *$p = 0.0351$). **O**, CNO (3 mg/kg) had no effect in a group of lesioned animals transfected with mCherry vector in the marble burying test (**O**, two-way repeated-measures ANOVA, nonsignificant effect of CNO, $F_{(1,5)} = 0.0002465$, $p = 0.9881$).

Pioneering studies have shown that the spontaneous activity of striatal neurons, which is highly dependent on cortical input (Wilson, 1993; Kasanetz et al., 2006), is increased in adult animals that have been depleted of nigrostriatal neurons early after birth (Onn et al., 1990). We do not find a significant change of the mean spontaneous firing rate of individual MSN, consistent with previous findings showing a higher number of spontaneously active striatal neurons without changes in their average firing rate (Galiñanes et al., 2009). This is in contrast to what happens in Parkinson's disease animal models, where the spontaneous activity of dMSN and iMSN is depressed and increased, respectively (Mallet et al., 2006; Ryan et al., 2018). These findings suggest a scenario where the dMSN hyperexcitability observed in the neonatal DAN lesion model may maintain or enhance positive thalamocortical feedback onto dMSN, resulting in preservation of spine density and responsiveness to PFC input despite the chronic dopamine depletion. In this context, preservation of locomotor activity may be the result of abnormal circuit maturation rather than of homeostatic mechanisms aimed at regulating behavioral output. This interpretation is consistent with the profound and lasting deficits observed in this animal model in the pattern of exploration of spatially complex environments, social behavior, and instrumental learning, despite the preservation of locomotor activity (Heffner and Seiden, 1983; Archer et al., 1988; Braz et al., 2015).

As shown by recent optogenetic and chemogenetic studies, instrumental learning and the explore/exploit balance depend on specific roles of dMSN and iMSN in monitoring and updating action selection and outcome values (Kravitz et al., 2012; Tai et al., 2012; Nonomura et al., 2018; Peak et al., 2020). These functions of MSN could be impaired by the changes in excitability and functional connectivity reported here. Indeed, the degree of anatomic segregation and overlap of cortical projections at the level of striatal subregions has long been considered of crucial importance for striatal function and learning (Haber, 2016; Marquand et al., 2017; Lee et al., 2019). Also, the timing of activation of dMSN and iMSN may be critical for movement control and learning (O'Hare et al., 2016, 2017). Speculatively, the dMSN hyperconnectivity and altered timing of dMSN and iMSN activations reported here, and the overall disorganization of frontostriatal responses reported in a previous study (Braz et al., 2015), could be responsible for the foraging deficits present in this animal model (Heffner and Seiden, 1983; Braz et al., 2015). In this sense, the chemogenetic inhibition aiming to acutely reduce dMSN hyperexcitability in the DMS of adult animals did not mitigate a characteristic behavioral impairment observed in these mice in the marble burying test, supporting that additional mechanisms contribute to this behavioral deficit. Studies in behaving animals are needed to determine how the changes in responsiveness to cortical input and input resistance observed in DAN-lesioned animals translate into striatal activity changes correlating to specific behavioral measures.

One unexpected finding of the present study is that both populations of MSN in the DMS seem to be homogeneous in terms of evoked activity and intrinsic excitability, by contrast to the functional differences observed in the DLS where dMSN respond more to their preferred input from the motor cortex (Escande et al., 2016) and are less excitable (Gertler et al., 2008) than iMSN. Further studies are needed to understand the underlying mechanisms and functional significance of these differences.

In conclusion, these results can shed light on the mechanisms underlying neuropsychiatric conditions, such as attention deficit hyperactivity disorder, autism, and Tourette syndrome, which have been linked to dopaminergic dysregulations in early postnatal life.

References

Albin RL, Young AB, Penney JB (1989) The functional anatomy of basal ganglia disorders. Trends Neurosci 12:366–375.

Alcacer C, Andreoli L, Sebastianutto I, Jakobsson J, Fieblinger T, Cenci MA (2017) Chemogenetic stimulation of striatal projection neurons modulates responses to Parkinson's disease therapy. J Clin Invest 127:720–734.

Archer T, Danysz W, Fredriksson A, Jonsson G, Luthman J, Sundström E, Teiling A (1988) Neonatal 6-hydroxydopamine-induced dopamine depletions: motor activity and performance in maze learning. Pharmacol Biochem Behav 31:357–364.

Ardayfio PA, Leung A, Park J, Hwang DY, Moran-Gates T, Choi YK, Carlezon JA, Tarazi FI, Kim KS (2010) Pitx3-deficient aphakia mice display unique behavioral responses to psychostimulant and antipsychotic drugs. Neuroscience 166:391–396.

Avale ME, Falzone TL, Gelman DM, Low MJ, Grandy DK, Rubinstein M (2004a) The dopamine D4 receptor is essential for hyperactivity and impaired behavioral inhibition in a mouse model of attention deficit/hyperactivity disorder. Mol Psychiatry 9:718–726.

Avale ME, Nemirovsky SI, Raisman-Vozari R, Rubinstein M (2004b) Elevated serotonin is involved in hyperactivity but not in the paradoxical effect of amphetamine in mice neonatally lesioned with 6-hydroxydopamine. J Neurosci Res 78:289–296.

Balleine BW (2019) The meaning of behavior: discriminating reflex and volition in the brain. Neuron 104:47–62.

Balleine BW, Dickinson A (1998) Goal-directed instrumental action: contingency and incentive learning and their cortical substrates. Neuropharmacology 37:407–419.

Biederman J, Faraone SV (2005) Attention-deficit hyperactivity disorder. Lancet 366:237–248.

Bowton E, Saunders C, Reddy IA, Campbell NG, Hamilton PJ, Henry LK, Coon H, Sakrikar D, Veenstra-VanderWeele JM, Blakely RD, Sutcliffe J, Matthies HJ, Erreger K, Galli A (2014) SLC6A3 coding variant Ala559Val found in two autism probands alters dopamine transporter function and trafficking. Transl Psychiatry 4:e464.

Braz BY, Galiñanes GL, Taravini IR, Belforte JE, Murer MG (2015) Altered corticostriatal connectivity and exploration/exploitation imbalance emerge as intermediate phenotypes for a neonatal dopamine dysfunction. Neuropsychopharmacology 40:2576–2587.

Bruno JP, Stricker EM, Zigmond MJ (1985) Rats given dopamine-depleting brain lesions as neonates are subsensitive to dopaminergic antagonists as adults. Behav Neurosci 99:771–775.

Castellanos FX (2002) Developmental trajectories of brain volume abnormalities in children and adolescents with attention-deficit/hyperactivity disorder. JAMA 288:1740.

Castellanos FX, Tannock R (2002) Neuroscience of attention-deficit/hyperactivity disorder: the search for endophenotypes. Nat Rev Neurosci 3:617–628.

Cepeda C, Walsh JP, Buchwald NA, Levine MS (1991) Neurophysiological maturation of cat caudate neurons: evidence from in vitro studies. Synapse 7:278–290.

Daw ND, Niv Y, Dayan P (2005) Uncertainty-based competition between prefrontal and dorsolateral striatal systems for behavioral control. Nat Neurosci 8:1704–1711.

del Río-Martín A, Pérez-Taboada I, Fernández-Pérez A, Moratalla R, de la Villa P, Vallejo M (2019) Hypomorphic expression of Pitx3 disrupts circadian clocks and prevents metabolic entrainment of energy expenditure. Cell Rep 29:3678–3692.e4.

Duncan GE, Criswell HE, McCown TJ, Paul IA, Mueller RA, Breese GR (1987) Behavioral and neurochemical responses to haloperidol and SCH-23390 in rats treated neonatally or as adults with 6-hydroxydopamine. J Pharmacol Exp Ther 243:1027–1034.

Durieux PF, Bearzatto B, Guiducci S, Buch T, Waisman A, Zoli M, Schiffmann SN, De Kerchove d'Exaerde A (2009) D2R striatopallidal neurons inhibit both locomotor and drug reward processes. Nat Neurosci 12:393–395.

Durston S, Fossella JA, Casey BJ, Hulshoff Pol HE, Galvan A, Schnack HG, Steenhuis MP, Minderaa RB, Buitelaar JK, Kahn RS, van Engeland H

(2005) Differential effects of DRD4 and DAT1 genotype on fronto-striatal gray matter volumes in a sample of subjects with attention deficit hyperactivity disorder, their unaffected siblings, and controls. Mol Psychiatry 10:678–685.

Eells JB, Lipska BK, Yeung SK, Misler JA, Nikodem VM (2002) Nurr1-null heterozygous mice have reduced mesolimbic and mesocortical dopamine levels and increased stress-induced locomotor activity. Behav Brain Res 136:267–275.

Escande MV, Taravini IR, Zold CL, Belforte JE, Murer MG (2016) Loss of homeostasis in the direct pathway in a mouse model of asymptomatic Parkinson's disease. J Neurosci 36:5686–5698.

Ferrari DC, Mdzomba BJ, Dehorter N, Lopez C, Michel FJ, Libersat F, Hammond C (2012) Midbrain dopaminergic neurons generate calcium and sodium currents and release dopamine in the striatum of pups. Front Cell Neurosci 6:7.

Fieblinger T, Graves SM, Sebel LE, Alcacer C, Plotkin JL, Gertler TS, Chan CS, Heiman M, Greengard P, Cenci MA, Surmeier DJ (2014a) Cell type-specific plasticity of striatal projection neurons in parkinsonism and L-DOPA-induced dyskinesia. Nat Commun 5:5316.

Fieblinger T, Sebastianutto I, Alcacer C, Bimpisidis Z, Maslava N, Sandberg S, Engblom D, Cenci MA (2014b) Mechanisms of dopamine D1 receptor-mediated ERK1/2 activation in the parkinsonian striatum and their modulation by metabotropic glutamate receptor type 5. J Neurosci 34:4728–4740.

Filali M, Lalonde R (2016) Neurobehavioral anomalies in the Pitx3/ak murine model of Parkinson's disease and MPTP. Behav Genet 46:228–241.

Fobbs WC, Bariselli S, Licholai JA, Miyazaki NL, Matikainen-Ankney BA, Creed MC, Kravitz AV (2020) Continuous representations of speed by striatal medium spiny neurons. J Neurosci 40:1679–1688.

Galiñanes GL, Taravini IR, Murer MG (2009) Dopamine-dependent periadolescent maturation of corticostriatal functional connectivity in mouse. J Neurosci 29:2496–2509.

Gerfen CR, Surmeier DJ (2011) Modulation of striatal projection systems by dopamine. Annu Rev Neurosci 34:441–466.

Gertler TS, Chan CS, Surmeier DJ (2008) Dichotomous anatomical properties of adult striatal medium spiny neurons. J Neurosci 28:10814–10824.

Gomez G, Escande MV, Suarez LM, Rela L, Belforte JE, Moratalla R, Murer MG, Gershanik OS, Taravini IR (2019) Changes in dendritic spine density and inhibitory perisomatic connectivity onto medium spiny neurons in l-Dopa-induced dyskinesia. Mol Neurobiol 56:6261–6275.

Graves SM, Surmeier DJ (2019) Delayed spine pruning of direct pathway spiny projection neurons in a mouse model of Parkinson's disease. Front Cell Neurosci 13:32.

Graybiel AM (2008) Habits, rituals, and the evaluative brain. Annu Rev Neurosci 31:359–387.

Haber SN (2016) Corticostriatal circuitry. Dialogues Clin Neurosci 18:7–21.

Hamilton PJ, Campbell NG, Sharma S, Erreger K, Herborg Hansen F, Saunders C, Belovich AN, Sahai MA, Cook EH, Gether U, McHaourab HS, Matthies HJ, Sutcliffe JS, Galli A, National Institutes of Health ARRA Autism Sequencing Consortium (2013) De novo mutation in the dopamine transporter gene associates dopamine dysfunction with autism spectrum disorder. Mol Psychiatry 18:1315–1323.

Hattori T, McGeer PL (1973) Synaptogenesis in the corpus striatum of infant rat. Exp Neurol 38:70–79.

Heffner TG, Seiden LS (1983) Impaired acquisition of an operant response in young rats depleted of brain dopamine in neonatal life. Psychopharmacology 79:115–119.

Hintiryan H, Foster NN, Bowman I, Bay M, Song MY, Gou L, Yamashita S, Bienkowski MS, Zingg B, Zhu M, Yang XW, Shih JC, Toga AW, Dong HW (2016) The mouse cortico-striatal projectome. Nat Neurosci 19:1100–1114.

Jin X, Costa RM (2015) Shaping action sequences in basal ganglia circuits. Curr Opin Neurobiol 33:188–196.

Kasanetz F, Riquelme LA, O'Donnell P, Murer MG (2006) Turning off cortical ensembles stops striatal Up states and elicits phase perturbations in cortical and striatal slow oscillations in rat in vivo. J Physiol 577:97–113.

Kozorovitskiy Y, Saunders A, Johnson C, Lowell BB, Sabatini BL (2012) Corrigendum: recurrent network activity drives striatal synaptogenesis. Nature 489:326.

Kravitz AV, Freeze BS, Parker PR, Kay K, Thwin MT, Deisseroth K, Kreitzer AC (2010) Regulation of parkinsonian motor behaviours by optogenetic control of basal ganglia circuitry. Nature 466:622–626.

Kravitz AV, Tye LD, Kreitzer AC (2012) Distinct roles for direct and indirect pathway striatal neurons in reinforcement. Nat Neurosci 15:816–818.

Larsen B, Olafsson V, Calabro F, Laymon C, Tervo-Clemmens B, Campbell E, Minhas D, Montez D, Price J, Luna B (2020) Maturation of the human striatal dopamine system revealed by PET and quantitative MRI. Nat Commun 11:846.

Lee CR, Yonk AJ, Wiskerke J, Paradiso KG, Tepper JM, Margolis DJ (2019) Opposing influence of sensory and motor cortical input on striatal circuitry and choice behavior. Curr Biol 29:1313–1323.e5.

Lieberman OJ, McGuirt AF, Mosharov EV, Pigulevskiy I, Hobson BD, Choi S, Frier MD, Santini E, Borgkvist A, Sulzer D (2018) Dopamine triggers the maturation of striatal spiny projection neuron excitability during a critical period. Neuron 99:540–554.e4.

Maia TV, Conceição VA (2018) Dopaminergic disturbances in Tourette syndrome: an integrative account. Biol Psychiatry 84:332–344.

Mallet N, Ballion B, Le Moine C, Gonon F (2006) Cortical inputs and GABA interneurons imbalance projection neurons in the striatum of parkinsonian rats. J Neurosci 26:3875–3884.

Marquand AF, Haak KV, Beckmann CF (2017) Functional corticostriatal connection topographies predict goal-directed behaviour in humans. Nat Hum Behav 1:0146.

Mazei-Robison MS, Couch RS, Shelton RC, Stein MA, Blakely RD (2005) Sequence variation in the human dopamine transporter gene in children with attention deficit hyperactivity disorder. Neuropharmacology 49:724–736.

Montague DM, Lawler CP, Mailman RB, Gilmore JH (1999) Developmental regulation of the dopamine D1 receptor in human caudate and putamen. Neuropsychopharmacology 21:641–649.

Montarolo F, Martire S, Perga S, Spadaro M, Brescia I, Allegra S, De Francia S, Bertolotto A (2019) NURR1 deficiency is associated to ADHD-like phenotypes in mice. Transl Psychiatry 9:207.

Nonomura S, Nishizawa K, Sakai Y, Kawaguchi Y, Kato S, Uchigashima M, Watanabe M, Yamanaka K, Enomoto K, Chiken S, Sano H, Soma S, Yoshida J, Samejima K, Ogawa M, Kobayashi K, Nambu A, Isomura Y, Kimura M (2018) Monitoring and updating of action selection for goal-directed behavior through the striatal direct and indirect pathways. Neuron 99:1302–1314.e5.

Nunes I, Tovmasian LT, Silva RM, Burke RE, Goff SP (2003) Pitx3 is required for development of substantia nigra dopaminergic neurons. Proc Natl Acad Sci USA 100:4245–4250.

O'Hare JK, Ade KK, Sukharnikova T, Van Hooser SD, Palmeri ML, Yin HH, Calakos N (2016) Pathway-specific striatal substrates for habitual behavior. Neuron 89:472–479.

O'Hare JK, Li H, Kim N, Gaidis E, Ade K, Beck J, Yin H, Calakos N (2017) Striatal fast-spiking interneurons selectively modulate circuit output and are required for habitual behavior. Elife 6:e26231.

Onn SP, Balzer JR, Sidney JP, Stricker EM, Zigmond MJ, Berger TW (1990) Lesions of the dopaminergic nigrostriatal system in neonatal rats: effects on the electrophysiological activity of striatal neurons recorded during adulthood. Brain Res 518:274–278.

Packard MG, Knowlton BJ (2002) Learning and memory functions of the basal ganglia. Annu Rev Neurosci 25:563–593.

Parker JG, Marshall JD, Ahanonu B, Wu YW, Kim TH, Grewe BF, Zhang Y, Li JZ, Ding JB, Ehlers MD, Schnitzer MJ (2018) Diametric neural ensemble dynamics in parkinsonian and dyskinetic states. Nature 557:177–182.

Paxinos G, Franklin KB (2004) The mouse brain in stereotaxic coordinates. Oxford, United Kingdom:Gulf Professional Publishing.

Peak J, Chieng B, Hart G, Balleine BW (2020) Striatal direct and indirect pathway neurons differentially control the encoding and updating of goal-directed learning. Elife 9:1–28.

Peixoto RT, Chantranupong L, Hakim R, Levasseur J, Wang W, Merchant T, Gorman K, Budnik B, Sabatini BL (2019) Abnormal striatal development underlies the early onset of behavioral deficits in Shank3B$^{-/-}$ mice. Cell Rep 29:2016–2027.e5.

Pennartz CM, Berke JD, Graybiel AM, Ito R, Lansink CS, van der Meer M, Redish D, Smith KS, Voorn P (2009) Corticostriatal interactions during learning, memory processing, and decision making. J Neurosci 29:12831–12838.

Pinault D (1996) A novel single-cell staining procedure performed in vivo under electrophysiological control: morpho-functional features of juxtacellularly labeled thalamic cells and other central neurons with biocytin or Neurobiotin. J. Neurosci Methods 65:113–136.

Plenz D, Kitai ST (1998) Up and down states in striatal medium spiny neurons simultaneously recorded with spontaneous activity in fast-spiking interneurons studied in cortex-striatum-substantia nigra organotypic cultures. J Neurosci 18:266–283.

Pomata PE, Belluscio M, Riquelme L, Murer MG (2008) NMDA receptor gating of information flow through the striatum in vivo. J Neurosci 28:13384–13389.

Roth BL (2016) DREADDs for neuroscientists. Neuron 89:683–694.

Ryan MB, Bair-Marshall C, Nelson AB (2018) Aberrant striatal activity in parkinsonism and levodopa-induced dyskinesia. Cell Rep 23:3438–3446.e5.

Sharpe NA, Tepper JM (1998) Postnatal development of excitatory synaptic input to the rat neostriatum: an electron microscopic study. Neuroscience 84:1163–1175.

Shaywitz B, Yager RD, Klopper JH (1976) Selective brain dopamine depletion in developing rats: an experimental model of minimal brain dysfunction. Science 191:305–308.

Shuen J, Chen M, Gloss B, Calakos N (2008) Drd1a-tdTomato BAC transgenic mice for simultaneous visualization of medium spiny neurons in the direct and indirect pathways of the basal ganglia. J Neurosci 28:2681–2685.

Stamford JA (1989) Development and ageing of the rat nigrostriatal dopamine system studied with fast cyclic voltammetry. J Neurochem 52:1582–1589.

Suarez LM, Alberquilla S, García-Montes JR, Moratalla R (2018) Differential synaptic remodeling by dopamine in direct and indirect striatal projection neurons in pitx3$^{-/-}$ mice, a genetic model of Parkinson's disease. J Neurosci 38:3619–3630.

Suárez LM, Solís O, Caramés JM, Taravini IR, Solís JM, Murer MG, Moratalla R (2014) L-DOPA treatment selectively restores spine density in dopamine receptor d2-expressing projection neurons in dyskinetic mice. Biol Psychiatry 75:711–722.

Tai LH, Lee AM, Benavidez N, Bonci A, Wilbrecht L (2012) Transient stimulation of distinct subpopulations of striatal neurons mimics changes in action value. Nat Neurosci 15:1281–1289.

Teicher MH, Andersen SL, Hostetter JC (1995) Evidence for dopamine receptor pruning between adolescence and adulthood in striatum but not nucleus accumbens. Dev Brain Res 89:167–172.

Tepper JM, Sharpe NA, Koós TZ, Trent F (1998) Postnatal development of the rat neostriatum: electrophysiological, light- and electron-microscopic studies. Dev Neurosci 20:125–145.

Tseng KY, Snyder-Keller A, O'Donnell P (2007) Dopaminergic modulation of striatal plateau depolarizations in corticostriatal organotypic cocultures. Psychopharmacology 191:627–640.

Van De Werd HJ, Uylings HB (2014) Comparison of (stereotactic) parcellations in mouse prefrontal cortex. Brain Struct Funct 219:433–459.

Vicente AM, Martins GJ, Costa RM (2020) Cortico-basal ganglia circuits underlying dysfunctional control of motor behaviors in neuropsychiatric disorders. Curr Opin Genet Dev 65:151–159.

Volkow ND, Wang GJ, Newcorn J, Telang F, Solanto MV, Fowler JS, Logan J, Ma Y, Schulz K, Pradhan K, Wong C, Swanson JM (2007) Depressed dopamine activity in caudate and preliminary evidence of limbic involvement in adults with attention-deficit/hyperactivity disorder. Arch Gen Psychiatry 64:932–940.

Voorn P, Kalsbeek A, Jorritsma-Byham B, Groenewegen HJ (1988) The pre- and postnatal development of the dopaminergic cell groups in the ventral mesencephalon and the dopaminergic innervation of the striatum of the rat. Neuroscience 25:857–887.

Voorn P, Vanderschuren LJ, Groenewegen HJ, Robbins TW, Pennartz CM (2004) Putting a spin on the dorsal-ventral divide of the striatum. Trends Neurosci 27:468–474.

Wall NR, DeLaParra M, Callaway EM, Kreitzer AC (2013) Differential innervation of direct- and indirect-pathway striatal projection neurons. Neuron 79:347–360.

Wilson CJ (1993) The generation of natural firing patterns in neostriatal neurons. Prog Brain Res 99:277–297.

Yin HH, Knowlton BJ (2006) The role of the basal ganglia in habit formation. Nat Rev Neurosci 7:464–476.

Yttri EA, Dudman JT (2016) Opponent and bidirectional control of movement velocity in the basal ganglia. Nature 533:402–406.